Human Molecular Genetics, 2017, Vol. 26, No. 9 1670–1677

doi: 10.1093/hmg/ddx073
Advance Access Publication Date: 1 March 2017
Original Article

ORIGINAL ARTICLE

Allele-specific ablation rescues electrophysiological abnormalities in a human iPS cell model of long-QT syndrome with a *CALM2* mutation

Yuta Yamamoto[1], Takeru Makiyama[1,*], Takeshi Harita[1], Kenichi Sasaki[1], Yimin Wuriyanghai[1,2], Mamoru Hayano[1], Suguru Nishiuchi[1], Hirohiko Kohjitani[1], Sayako Hirose[1], Jiarong Chen[1], Fumika Yokoi[1], Taisuke Ishikawa[3], Seiko Ohno[2], Kazuhisa Chonabayashi[4], Hideki Motomura[5], Yoshinori Yoshida[4,*], Minoru Horie[2], Naomasa Makita[3,*] and Takeshi Kimura[1]

[1]Department of Cardiovascular Medicine, Kyoto University Graduate School of Medicine, Sakyo-ku, Kyoto 606-8507, Japan, [2]Department of Cardiovascular and Respiratory Medicine, Shiga University of Medical Science, Seta-Tsukinowa, Otsu 520-2192, Japan, [3]Department of Molecular Physiology, Nagasaki University Graduate School of Biomedical Sciences, Nagasaki 852-8523, Japan, [4]Department of Life Science Frontiers, Center for iPS Cell Research and Application, Kyoto University, Sakyo-ku, Kyoto 606-8507, Japan and [5]Department of Pediatrics, Nagasaki University Hospital, Nagasaki 852-8501, Japan

*To whom correspondence should be addressed at: Department of Cardiovascular Medicine, Kyoto University Graduate School of Medicine, 54 Shogoin Kawahara-cho, Sakyo-ku, Kyoto 606-8507, Japan. Tel: +81 757513196; Fax: +81 757513289; Email: makiyama@kuhp.kyoto-u.ac.jp (T.M.); Department of Life Science Frontiers, Center for iPS Cell Research and Application, Kyoto University, 53 Shogoin Kawahara-cho, Sakyo-ku, Kyoto 606-8507, Japan. Tel: +81 753667000; Fax: +81 753667023; Email: yoshinor@cira.kyoto-u.ac.jp (Y.Y.); Department of Molecular Physiology, Nagasaki University Graduate School of Biomedical Sciences, 1-12-4 Sakamoto, Nagasaki 852-8523, Japan. Tel: +81 958197031; Fax: +81 958197911; Email: makitan@nagasaki-u.ac.jp (N.M.)

Abstract

Calmodulin is a ubiquitous Ca^{2+} sensor molecule encoded by three distinct calmodulin genes, *CALM1–3*. Recently, mutations in *CALM1–3* have been reported to be associated with severe early-onset long-QT syndrome (LQTS). However, the underlying mechanism through which heterozygous calmodulin mutations lead to severe LQTS remains unknown, particularly in human cardiomyocytes. We aimed to establish an LQTS disease model associated with a *CALM2* mutation (LQT15) using human induced pluripotent stem cells (hiPSCs) and to assess mutant allele-specific ablation by genome editing for the treatment of LQT15. We generated LQT15-hiPSCs from a 12-year-old boy with LQTS carrying a *CALM2*-N98S mutation and differentiated these hiPSCs into cardiomyocytes (LQT15-hiPSC-CMs). Action potentials (APs) and L-type Ca^{2+} channel (LTCC) currents in hiPSC-CMs were analyzed by the patch-clamp technique and compared with those of healthy controls. Furthermore, we performed mutant allele-specific knockout using a CRISPR-Cas9 system and analyzed electrophysiological properties. Electrophysiological analyses revealed that LQT15-hiPSC-CMs exhibited significantly lower beating rates, prolonged AP durations, and impaired inactivation of LTCC currents compared with control cells, consistent with clinical phenotypes. Notably, ablation of the mutant allele rescued the electrophysiological abnormalities of LQT15-hiPSC-CMs, indicating that the mutant

Received: December 7, 2016. **Revised:** February 3, 2017. **Accepted:** February 22, 2017

allele caused dominant-negative suppression of LTCC inactivation, resulting in prolonged AP duration. We successfully recapitulated the disease phenotypes of LQT15 and revealed that inactivation of LTCC currents was impaired in *CALM2*-N98S hiPSC model. Additionally, allele-specific ablation using the latest genome-editing technology provided important insights into a promising therapeutic approach for inherited cardiac diseases.

Introduction

Congenital long-QT syndrome (LQTS) is a genetic disorder characterized by a prolonged cardiac repolarization phase resulting in a long QT interval in the electrocardiogram (ECG). LQTS can cause syncope and even sudden death during early development. To date, 15 LQTS subtypes caused by mutations in genes encoding ion channels or channel regulators have been reported (1–4).

Recently, mutations in *CALM* genes, which encode the ubiquitous Ca^{2+} sensor calmodulin (CaM), have been reported to be associated with severe early-onset LQTS (LQT14 and -15) (5,6), catecholaminergic polymorphic ventricular tachycardia (CPVT) (7), and familial idiopathic ventricular fibrillation (8). Three distinct genes (*CALM1*, *CALM2*, and *CALM3*) encode an identical CaM protein in humans. CaM modulates various proteins including several ion channels (9–12), sarcoplasmic reticulum ryanodine receptor/Ca^{2+} release channels (RyR2) (13,14), and Ca^{2+}/CaM-dependent protein kinase (CaMKll) (15). Particularly during the regulation of L-type Ca^{2+} channels (LTCCs), the complex of Ca^{2+}-CaM promotes inactivation of LTCC currents (I_{CaL}) (16).

Human induced pluripotent stem cell (hiPSC) technology is a powerful tool for studying inherited diseases in humans, and several cardiac diseases have been investigated using hiPSC-derived cardiomyocytes (hiPSC-CMs) (17–19). In most human arrhythmias, rodents cannot serve as an efficient model because their cardiac electrophysiological properties are distinct from those of humans; that is, rodent exhibit a faster heart rate and shorter action potential (AP) due to variations in ion channel gene expression (20,21).

CaM variants associated with LQTS and CPVT have been suggested to exert a dominant-negative effect on wild-type (WT) CaMs because heterozygous mutations in one of three *CALM* genes cause severe phenotypes though WT CaMs produced from the other five alleles. Therefore, because mutant CaMs can cause dominant-negative suppression of wild-type CaMs as a putative mechanism in LQT15, allele-specific ablation using a clustered regularly interspaced short palindromic repeat (CRISPR) and CRISPR-associated 9 (Cas9) endonuclease system may allow rescue of the electrophysiological abnormalities observed in LQT15-hiPSC-CMs.

In this study, we established a hiPSC model from a patient with LQTS carrying a heterozygous *CALM2*-N98S mutation and successfully recapitulated the disease phenotypes. In addition, we conducted genome editing of LQT15-hiPSCs using the CRISPR-Cas9 system and rescued the observed electrophysiological abnormalities. Our findings provide important insights into the pathophysiological mechanisms of this disease and offer a promising therapeutic approach for *CALM*-related LQTS.

Results

Generation of LQT15-hiPSCs

Patient-specific LQT15-hiPSCs were generated from the peripheral blood mononuclear cells of a 12-year-old boy with LQTS carrying a heterozygous *CALM2* mutation (c.293A > G, p.N98S), whose clinical features were described previously (5). He had episodes of syncope, and his ECG showed a mildly prolonged QT interval at rest (QTc 478 ms). The epinephrine infusion test evoked pronounced QT prolongation. There was no family history of arrhythmia or sudden death (5). We obtained peripheral blood mononuclear cells from the index patient after written informed consent, and hiPSCs were generated using an integration-free episomal vector method (22). As a control, 201B7 and 253G1 hiPSC lines generated from a healthy individual were used in this study (23,24). The LQT15-hiPSCs showed characteristics of human embryonic stem cell morphology and stained positive for pluripotency markers (Fig. 1A). We confirmed the expected mutation, *CALM2*-N98S, in LQT15-hiPSC clones but not in the control (Fig. 1B).

Mutated CaM ablation using an allele-specific CRISPR-Cas9 nickase system in LQT15-hiPSCs

In order to ablate mutated CaMs in LQT15-hiPSCs, we designed target vectors using a web-based program (http://crispr.mit.edu/; date last accessed March 8, 2017; Fig. 2A), and LQT15-hiPSCs were transfected with a Cas9 nickase/guide RNA (gRNA) expression vector. After puromycin selection, we isolated 18 clones and screened them by sequencing (Supplementary Material, Table S1). Consequently, we obtained two clones with

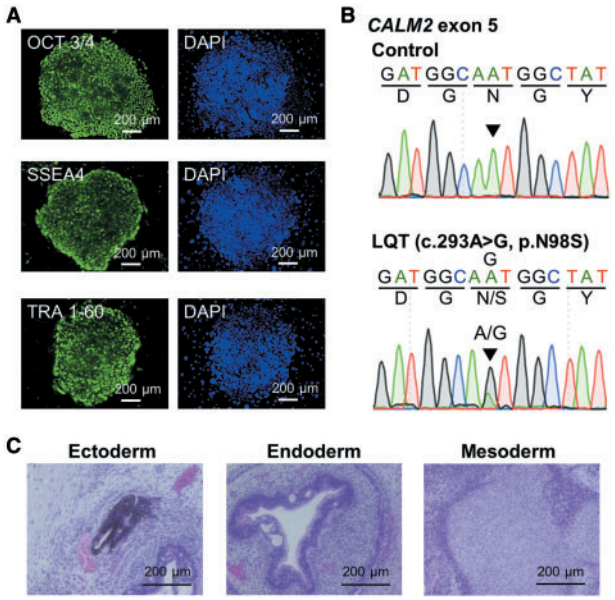

Figure 1. Characterization of LQT15-hiPSCs. (**A**) LQT15-hiPSC colonies derived from the peripheral blood mononuclear cells of a patient with LQTS expressed pluripotency markers, as shown by immunostaining. Scale bars = 200 μm. (**B**) Sequencing analysis of the *CALM2* gene identified the p.N98S (c.293A>G) heterozygous mutation in the LQT15-hiPSCs. (**C**) Hematoxylin-eosin staining of teratomas formed from LQT15-iPSCs showed differentiation of the cells into various tissues derived from all three germ layers: melanocytes (ectoderm), gut-like structures (endoderm), and cartilage tissue (mesoderm). Scale bars = 200 μm.

mutant allele-specific knockout (LQT15-KO clones 1 and 2; Fig. 2B). These clones carried out-of-frame mutations and were expected to produce a premature stop codon. LQT15-KO-hiPSC1 carried a 5-bp deletion from intron 4 to exon 5 (4 bp in intron 4 and 1 bp in exon 5). This mutation was thought to lead to exon skipping and produced a stop codon after the amino acid residues. LQT15-KO-hiPSC2 carried a 38-bp insertion in exon 5, resulting in a frame-shift mutation and premature stop codon at residue 98. In these clones, we checked for the potential off-target mutations in the top 5 predicted candidate sites identified using bioinformatics programs by sequencing and did not detect any genome modifications. We conducted quantitative real-time polymerase chain reaction (PCR) in hiPSC-CMs and found that *CALM2* expression in LQT15-KO-hiPSC-CMs was approximately half that in LQT15-hiPSC-CMs (Fig. 3A).

Allele-specific ablation rescued the abnormal electrophysiological properties of LQT15-hiPSC-CMs

We differentiated hiPSCs into CMs using the embryoid body (EB) formation method (25). The beating rate of LQT15-EBs was significantly lower than that of the control, and it was rescued in LQT15-KO-EBs (LQT15: 24.2 ± 1.3 bpm, control: 47.3 ± 1.7 bpm, LQT15-KO: 40.9 ± 2.0 bpm; $P < 0.01$, LQT15 vs control or LQT15-KO; Fig. 3B). Spontaneous APs were recorded from single hiPSC-CMs using the current-clamp technique. APs in hiPSC-CMs have been reported to have various morphologies that can be categorized as ventricular-, atrial-, or nodal-like. In the present study, we analyzed ventricular-like cells categorized based on previously reported criteria (26,27). Typical ventricular-type APs are shown in Figure 4A. In agreement with the results observed in EBs, the frequency of spontaneous APs in LQT15-hiPSC-CMs was significantly lower than that in control- and LQT15-KO-hiPSC-CMs (LQT15: 30.8 ± 5.5 bpm, control: 79.4 ± 17.2 bpm, LQT15-KO: 83.9 ± 10.8 bpm; $P < 0.05$, LQT15 vs control; $P < 0.01$, LQT15 vs LQT15-KO; Supplementary Material, Table S2). AP durations (APDs) at 50% and 90% repolarization (APD_{50} and APD_{90}) were significantly prolonged in LQT15-hiPSC-CMs compared with those in control (APD_{50} and APD_{90}: LQT15, 663.5 ± 94.8 ms and 790.6 ± 101.0 ms, respectively, vs control, 224.6 ± 20.4 ms and 276.3 ± 24.5 ms, respectively; $P < 0.01$; Fig. 4B, Supplementary Material, Table S2). Allele-specific ablation ameliorated prolonged APD of LQT15-hiPSC-CMs. The APD_{50} and APD_{90} of LQT15-KO-hiPSC-CMs (252.8 ± 20.8 ms and 326.1 ± 28.6 ms, respectively) were significantly shorter than those of LQT15-hiPSC-CMs (Fig. 4B, Supplementary Material, Table S2). Because APD was affected by beating rate, we corrected APD_{50} and APD_{90} ($cAPD_{50}$ and $cAPD_{90}$) by following equation: $APD/(\text{spontaneous cycle length})^{1/2}$ as previously reported (28,29). Even after adjustment for beating intervals, the $cAPD_{50}$ and $cAPD_{90}$ of LQT15-hiPSC-CMs were also significantly prolonged compared with those of the control, and it was rescued in LQT15-KO-hiPSC-CMs to a similar level as in control-hiPSC-CMs ($cAPD_{50}$ and $cAPD_{90}$: LQT15, 403.2 ± 53.8 ms and 484.3 ± 63.2 ms, respectively, control, 213.0 ± 18.2 ms and 263.3 ± 22.3 ms, respectively, LQT15-KO, 283.6 ± 20.7 ms and 361.6 ± 29.2 ms, respectively; $P < 0.01$, LQT15 vs control; $P < 0.05$, LQT15 vs LQT15-KO; Fig. 4C, Supplementary Material, Table S2). In LQT15-KO-hiPSC-CMs, maximum diastolic membrane potentials were significantly more depolarized than control- and LQT15-hiPSC-CMs (LQT15-KO: -59.8 ± 1.6 mV, control:-69.7 ± 1.9 mV, LQT15: -72.6 ± 2.8 mV; $P < 0.01$, LQT15-KO vs control or LQT15; Supplementary Material, Table S2); however, there were no significant differences in any other AP parameters (Supplementary Material, Table S2).

Using the voltage-clamp technique, we recorded I_{CaL} of control-, LQT15-, and LQT15-KO-hiPSC-CMs (Fig. 5A and B). Notably, inactivation of LTCCs was impaired in LQT15-hiPSC-CMs compared with that in control cells. The time constants of inactivation in LQT15-hiPSC-CMs were significantly larger than those of the control (Fig. 5C). Figure 5D shows the ratio of I_{CaL} remaining after 100-ms depolarization to the peak current (r100). The values of r100 in LQT15-hiPSC-CMs were also significantly larger than those of the control (Fig. 5D). There were no significant differences between control- and LQT15-hiPSC-CMs in the current-voltage relationship and conductance-voltage activation and inactivation curves (Fig. 5E and F, Supplementary Material, Table S3). In LQT15-KO-hiPSC-CMs, the inactivation of LTCCs was improved (Fig. 5C and D). The time constants of inactivation and the value of r100 in LQT15-KO-hiPSC-CMs were significantly smaller than those of LQT15-hiPSC-CMs (Fig. 5C and D). In comparison to control, r100 of LQT15-KO-hiPSC-CMs was significantly larger at -10 and 0 mV. The k value of the activation curve in LQT15-KO-hiPSC-CMs was significantly larger than that in control- and LQT15-hiPSC-CMs (Supplementary Material, Table S3).

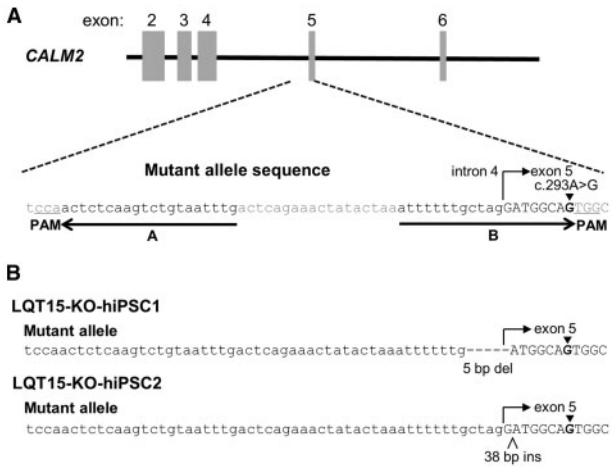

Figure 2. Mutant allele ablation in LQT15-hiPSC-CMs. (**A**) Design of a pair of guide RNAs (gRNAs) for mutant allele-specific knockout. The uppercase letters indicate the sequence of exon 5 in *CALM2*. The PAM sequence is underlined, and the c.293A>G point mutation is indicated in bold. (**B**) Sequences of the LQT15-KO iPSC clones.

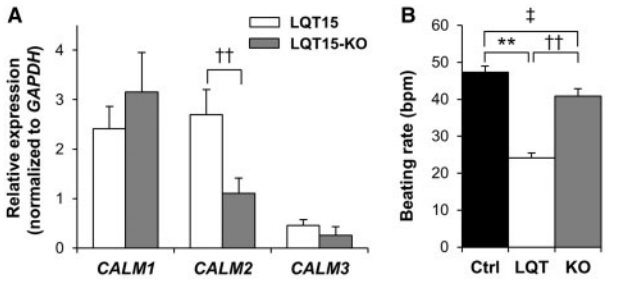

Figure 3. *CALM* expression and beating rate of hiPSC embryoid bodies. (**A**) Quantitative PCR analysis of gene expression of *CALM1-3* in LQT15- ($n = 5$) and LQT15-KO-hiPSC-CMs ($n = 4$). (**B**) The beating rates of control- ($n = 58$), LQT15- ($n = 62$), and LQT15-KO embryoid bodies ($n = 62$). $^{**}P < 0.01$ (Control vs LQT15). $^{††}P < 0.01$ (LQT15 vs LQT15-KO). $^{‡}P < 0.05$ (LQT15-KO vs Control).

Discussion

iPSC technology offers a unique opportunity to establish cellular models of disease for investigation of the underlying pathological mechanisms. In this study, we established a patient-derived iPSC-based model of LQTS associated with the *CALM2*-N98S mutation and successfully recapitulated the phenotypes, i.e., a lower beating rate and longer APD, consistent with the clinical phenotype of the index patient with bradycardia and a prolonged QTc interval (5). In addition, we performed mutant allele-specific ablation in LQT15-hiPSCs using the CRISPR-Cas9 system, which resulted in attenuation of the abnormal electrophysiological properties of the cells, indicating a dominant negative effect of *CALM2*-N98S.

CaM is comprised of N- and C-terminal lobes, and each lobe of CaM contains two EF hands as Ca^{2+} binding motifs. The Ca^{2+} binding affinity of the EF hands has been reported to be higher in the C-terminal lobe compared with that in the N-terminal lobe (30). Interestingly, most mutations identified in patients with CaM-related LQTS are located in EF hands in the C-lobe (5,6). Mutant CaMs associated with LQTS have been reported to exhibit low Ca^{2+} binding affinity compared with that of WT CaMs (5,6); however, the Ca^{2+} binding affinity of CPVT mutant CaMs is not significantly different compared to that of WT CaMs (7,31). CaM plays an important role in many cardiac ion channels (9,14,32,33); in particular, inactivation of LTCC is promoted by the interaction between the complex of Ca^{2+}-CaMs and the IQ motif in the C-terminus of LTCC (32). Thus, the low Ca^{2+} binding affinity of mutant CaMs may impair LTCC inactivation. The mutant CaM N98S was reported to have lower Ca^{2+} binding affinity than WT CaM (7,31), and Limpitikul *et al.* (34) reported that overexpressed N98S-CaM in guinea pig cardiomyocytes exhibited prolonged APDs and impaired LTCC inactivation, consistent with our results in the LQT15-hiPSC model. Regarding the assessment of APD during spontaneous beating in hiPSC-CMs, we corrected APD by Bazett's formula according to previous reports (28,29). However, the method to correct APD appropriately *in vitro* model is not established and further investigations will be needed.

CaM also regulates RyR2 channels (14,31,35). WT CaMs bind RyR2 channels, decreasing the RyR2 channel open probability (14). In 2012, Nyegaard *et al.* described CPVT cases associated with *CALM1* mutations (N54I and N98S) and showed an impaired binding affinity to RyR2 peptides in N98S but not N54I under low Ca^{2+} conditions (7). In contrast, Hwang *et al.* showed that the CPVT-related mutant CaMs N54I and N98S exhibited higher binding affinity to RyR2 channels than WT CaMs in sarcoplasmic reticulum vesicles prepared from the porcine ventricular myocardium (31). In their study, N54I and N98S mutant CaMs increased the single channel open probability of RyR2 channels in artificial lipid bilayers and increased the Ca^{2+} wave frequency in mouse ventricular CMs. Currently, the interaction between CPVT-related mutant CaMs and RyR2 channels remains controversial. Similarly, it is unclear why the *CALM2*-N98S mutant in our case did not exhibit typical CPVT phenotypes, despite the observation that the N98S mutation in *CALM1*, which produces the same amino acid sequence, is

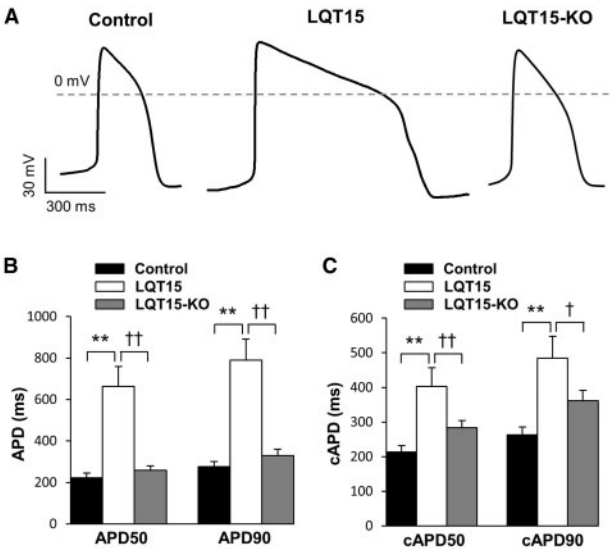

Figure 4. Mutant allele ablation can rescue electrophysiological abnormalities in LQT15-hiPSC-CMs. (**A**) Typical ventricular-type action potential waveforms of control-, LQT-15-, and LQT15-KO-hiPSC-CMs during spontaneous beating. (**B**) The action potential duration (APD) of control- ($n = 11$), LQT15- ($n = 8$), and LQT15-KO-hiPSC-CMs ($n = 10$) measured at 50% and 90% repolarization (APD_{50} and APD_{90}) from the AP peak of spontaneous ventricular-type APs. (**C**) Corrected APD_{50} and APD_{90} according to beating rate ($cAPD_{50}$ and $cAPD_{90}$). $^{**}P < 0.01$ (Control vs LQT15). $^{\dagger}P < 0.05$, $^{\dagger\dagger}P < 0.01$ (LQT15 vs LQT15-KO).

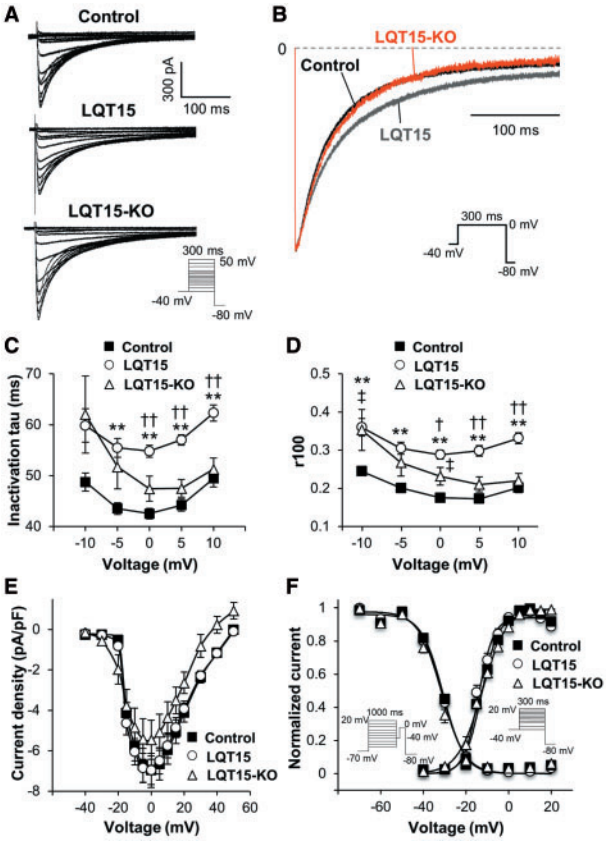

Figure 5. Functional analysis of L-type calcium channels (LTCCs). (**A**) Representative I_{CaL} traces in control-, LQT15-, and LQT15-KO-hiPSC-CMs were elicited by the protocol shown in the inset. (**B**) Normalized I_{CaL} traces in control-, LQT15-, and LQT15-KO-hiPSC-CMs. (**C**) The time constants of inactivation in control-, LQT15, and LQT15-KO-hiPSC-CMs. (**D**) The ratio of peak current remaining after 100 ms depolarization to the peak current (r100). (**E**) Peak inward current-voltage relationship of the control- ($n = 12$), LQT15- ($n = 13$), and LQT15-KO-hiPSC-CMs ($n = 7$). The peak inward current was normalized to the cell capacitance to give the I_{CaL}. (**F**) Steady-state inactivation and activation of control-, LQT15-, and LQT15-KO-hiPSC-CMs were plotted. $^{**}P < 0.01$ (Control vs LQT15). $^{\dagger}P < 0.05$, $^{\dagger\dagger}P < 0.01$ (LQT15 vs LQT15-KO). $^{\ddagger}P < 0.05$ (LQT15-KO vs Control).

associated with CPVT (7). We assume that different expression levels of *CALM1* and *CALM2* in specific cell types may be associated with different phenotypes in these two cases.

In addition to RyR2, CaM is known to regulate other cardiac ion channels, such as voltage-gated Na^+ channels (Nav1.5) and voltage-gated K^+ channels ($K_v7.1$), which have the potential to contribute to APD prolongation. Inactivation of Nav1.5 is regulated by CaM, and ablation of this regulation results in Nav1.5 dysfunction (33,36). With regard to LQTS-mutant CaMs, Yin *et al.* studied whether D96V-, D130G-, and F142L-CaMs affected late Na^+ currents in a heterologous expression system or mouse ventricular myocytes and concluded that Nav1.5 dysfunction was not the major cause of LQTS associated with CaM mutations (37). Further studies are needed to investigate the interaction between N98S mutant CaMs and Nav1.5.

Kv7.1 (I_{Ks}), encoded by *KCNQ1*, plays an important role in the repolarization of cardiomyocytes and requires CaM for assembly and correct gating (9,10,38). Shamgar *et al.* reported that *KCNQ1* mutations located near the IQ motif impair CaM binding, confer inactivation, and reduce I_{Ks} current amplitude (9). Therefore, reduction of CaM binding affinity to Kv7.1 may decrease the density of I_{Ks} and prolong APD in LQTS-related CaM mutations. Other molecular targets of CaM, including CaMKll and HCN4 channels, are considered potential contributors to LQT15 phenotypes (39,40). Additional investigations may provide insights into the contributions of these targets to the underlying mechanisms of LQT15 phenotypes.

The CRISPR-Cas9 system has proven to be an efficient genome editing tool in iPSCs and is useful for creating gene KO or knock-in hiPSCs (41,42). Moreover, this system has the potential to correct genetic mutations in hiPSC-related disease models (43–45). However, compared with other recent approaches involving targeted genome modification, the CRISPR-Cas9 system has a higher occurrence of off-target effects (46,47). To improve the specificity of Cas9-mediated genome editing, a Cas9 double nickase system was reported to minimize the off-target effects of this system (48). Here, we successfully performed allele-specific KO using the Cas9 double nickase system without any unwanted genome modifications in the other putative targets; this strategy rescued the abnormal electrophysiological properties of LQT15-hiPSC-CMs. Considering that an identical CaM protein is expressed from three distinct genes, Limpitikul *et al.* recently reported that transcriptional repression of *CALM2* using CRISPR interference which nonspecifically targeted both WT and mutant alleles ameliorated the prolonged APDs in the patient-specific iPSC model (49). In contrast with their strategy, our allele-specific ablation does not affect the expression of WT allele and is also applicable to other diseases caused by a dominant negative mechanism. However, we need to take care of the effect of one *CALM2* allele knockout on cardiomyocytes. LQT15-KO-iPSC-CMs exhibited different electrophysiological properties in maximum diastolic potential, r100, and the slope factor k in steady-state activation from control-hiPSC-CMs. Therefore, further investigations will be required for elucidating the mechanisms underlying these alterations in LQT15-KO-hiPSC-CMs. Regarding *in vivo* genome editing, Nelson *et al.* and Tabebordber *et al.* performed in a DMD mouse model using a small, efficient Cas9 with an adeno-associated virus delivery system (50,51). Additional improvements to genome editing are needed to enhance the safety, specificity, and efficiency of this method, in conjunction with better delivery technologies, in order to target organs for efficient gene therapy in the clinical setting.

Conclusion

Here, we established disease-specific iPSC clones from an individual with LQTS carrying a *CALM2*-N98S mutation as an *in vitro* disease model, which recapitulated the LQT15 phenotype. Additionally, we found that inactivation of LTCCs was impaired in LQT15-hiPSC-CMs, resulting in APD prolongation. Using the Cas9 double nickase system, we performed allele-specific ablation in LQT15-hiPSCs, rescuing the abnormal electrophysiological properties in LQT15-hiPSC-CMs. These findings demonstrated the additional evidence of a dominant-negative effect of *CALM2*-N98S and indicated that this therapeutic approach has potential for the treatment of diseases caused by dominant-negative mechanisms. This hiPSC-based disease model provides a powerful platform for studying the pathophysiological mechanisms of LQTS and for developing novel therapies for this disorder.

Materials and Methods

hiPSC generation and cardiomyocyte differentiation

After obtaining informed consent, hiPSCs were generated from the peripheral blood mononuclear cells of the index patient using an integration-free episomal vector method (22). As a control, 201B7 and 253G1 hiPSC lines generated from a healthy individual were used in this study (23,24). We differentiated hiPSCs into cardiomyocytes using an EB differentiating system (25). During cardiac differentiation, cells were incubated at 37°C in 5% CO_2, 5% O_2, and 90% N_2 for the first 12 days to promote differentiation. The hiPSCs aggregated to form EBs and were cultured in suspension for 20 days. On the 20th day of culture, EBs were treated with collagenase B (Roche, Basel, Switzerland) and trypsin EDTA (Nacalai Tesque, Kyoto, Japan) and dispersed into single cells or small clusters, which were plated onto 0.1% gelatin-coated dishes. hiPSC-CMs were then maintained in conditioned medium. This study was approved by the Kyoto University ethics review board (G259) and conformed to the principles of the Declaration of Helsinki.

Genome sequencing

Genomic DNA was isolated from hiPSCs by GenElute Mammalian Genomic DNA Miniprep kit (Sigma-Aldrich, St Louis, MO, USA). Purified DNA was amplified with specific primers and analyzed by Genetic Analyzer 3130 and Big Dye Terminater v3.1 (Thermo Fisher Scientific, Waltham, MA, USA). Primers are described in Supplementary Material, Table S5.

Immunostaining

For immunostaining, hiPSC colonies were fixed with 4% paraformaldehyde. The cells were permeabilized by 0.2% TritonX-100 (Nacalai Tesque). The samples were stained with the following primary antibodies: mouse monoclonal anti-OCT3/4 (1:50; Santa Cruz Biotechnology, Dallas, TX, USA), mouse monoclonal anti-SSEA4 (1:200; Santa Cruz Biotechnology), and mouse monoclonal anti-TRA 1-60 (1:200; Santa Cruz Biotechnology). The secondary antibody was donkey anti-mouse Alexafluor 488 (1:1000, Thermo Fisher Scientific). The nuclei were stained with DAPI (1:2000, Wako Pure Chemical Industries, Osaka, Japan). The specimens were observed under a fluorescence microscope, Biozero BZ-9000 (Keyence, Osaka, Japan).

Teratoma formation

The hiPSCs were injected into scid/scid mice under the testis. Tumor samples were collected at 8 weeks, fixed in 10% formalin, and stained with hematoxylin and eosin.

CRISPR Cas9 nickase vector and guide RNA design

We used the PX462 (Addgene plasmid #62987) (52) for Cas9 double nickase system, which is an expression vector encoding Cas9 nickase and gRNA. The gRNAs were designed for targeting of the exon 5 in the *CALM2* gene, and one gRNA was designed for mutant allele specific sequence. The sequences were described in Figure 2A.

Transfection of CRISPR into LQT15-hiPSCs

hiPSCs were washed with PBS and treated with CTK solution (ReproCell, Yokohama, Japan) for 30-40 sec at 37°C to remove feeders. The cells were washed twice with PBS. To obtain single cell, the cells were further dissociated by Accumax (Innovative Cell Technologies, San Diego, CA, USA) solution for 10 min at 37°C and neutralized with culture medium. Single cells were transfected with CRISPR-Cas9 nickase vectors (1.25 μg guide A and 1.25 μg guide B) using Lipofectamine 3000 (Thermo Fisher Scientific) and plated at densities of 0.8×10^6 cells per well in matrigel coated 6-well plate in the presence of 10 μM Y-27632 (Wako Pure Chemical Industries). Starting 2 days after transfection, we conducted the selection of the transfected colonies by puromycin (1 μg/ml) for 48 h. The transfected colonies were picked up at 7 days after puromycin-selection.

Analysis of off-target effects

The potential off-target loci were predicted using bioinformatics programs (47). Sanger sequencing across the regions of top 5 loci (Supplementary Material, Table S4) for each gRNA was performed. The primers for amplifying and sequencing the off-target loci are listed in Supplementary Material, Table S5.

Quantitative PCR

Total RNAs were isolated using TRIzol Reagent (Thermo Fisher Scientific) from beating EBs microdissected from hiPSC-CMs on the 30th day. These RNAs were treated with TURBO DNA-free Kit (Thermo Fisher Scientific) and transcribed into complementary DNA (cDNA) by using Transcriptor First Strand cDNA Synthesis Kit (Roche). The primers used in this study are described in Supplementary Material, Table S5. The quantitative PCR (qPCR) was performed using a Taqman method. The expression of genes were normalized relative to *GAPDH* and assessed using the comparative change in the threshold cycle (ΔC_t) method.

Electrophysiological analysis

Data were acquired at 10 kHz with the Multiclamp 700B amplifier (Molecular Devices, Sunnyvale, CA, USA), Digidata 1440 digitizer hardware (Molecular Devices) and pClamp 10.4 software (Molecular Devices) on experimental requirements. Plated hiPSC-CMs 5 to 8 weeks after differentiation were dissociated as above to record AP and I_{CaL}. For single cell patch-clamp recordings, gelatin-coated glass coverslips were placed into each well of a 6-well plate, and 2 ml of DMEM/F12 containing 2% FBS and 80,000-120,000 cardiomyocytes were added in each well. Spontaneous APs were recorded from spontaneously beating single cardiomyocytes by using the perforated patch-clamp technique with amphotericin B (Sigma-Aldrich) at 36 ± 1°C. I_{CaL} recordings were performed by whole-cell voltage-clamp at 25 ± 1°C. Experimental details regarding measurements of APs and I_{CaL}, as well as data analysis methods, in hiPSC-CMs are described in the Supplemental Material.

Statistical Analysis

All data were shown as mean ± SEM. Statistical significance was defined as $P < 0.05$. Statistical significance was evaluated by using one-way ANOVA followed by Tukey's test. qPCR data were analyzed by Student's *t*-tests.

Supplementary Material

Supplementary Material is available at *HMG* online.

Acknowledgements

T.M. was supported by JSPS KAKENHI and Suzuken Memorial Foundation, T.K. was supported by Suzuken Memorial Foundation, and N.M. was supported by Grant-in-Aid for Scientific Research from the Ministry of Education, Culture, Sports, Science and Technology, and research grant from the Japan Agency for Medical Research and Development and AMED.
We thank Masako Tanaka, Aya Umehara, and Kyoko Yoshida for their technical assistance.

Conflict of Interest statement. Y.Y. owns stock in iPS Portal.

Funding

JSPS KAKENHI (grant number 25461054), Suzuken Memorial Foundation, Grant-in-Aid for Scientific Research (grant no. 15H04823) from the Ministry of Education, Culture, Sports, Science and Technology, and research grant from the Japan Agency for Medical Research and Development, AMED (grant no. 15km0305015h0101).

References

1. Curran, M.E., Splawski, I., Timothy, K.W., Vincent, G.M., Green, E.D. and Keating, M.T. (1995) A molecular basis for cardiac arrhythmia: HERG mutations cause long QT syndrome. *Cell*, **80**, 795–803.
2. Wang, Q., Curran, M.E., Splawski, I., Burn, T.C., Millholland, J.M., VanRaay, T.J., Shen, J., Timothy, K.W., Vincent, G.M., de Jager, T., *et al.* (1996) Positional cloning of a novel potassium channel gene: KVLQT1 mutations cause cardiac arrhythmias. *Nat. Genet.*, **12**, 17–23.
3. Wang, Q., Shen, J., Splawski, I., Atkinson, D., Li, Z., Robinson, J.L., Moss, A.J., Towbin, J.A. and Keating, M.T. (1995) SCN5A mutations associated with an inherited cardiac arrhythmia, long QT syndrome. *Cell*, **80**, 805–811.
4. Mizusawa, Y., Horie, M. and Wilde, A.A.M. (2014) Genetic and clinical advances in congenital long QT syndrome. *Circ. J.*, **78**, 2827–2833.
5. Makita, N., Yagihara, N., Crotti, L., Johnson, C.N., Beckmann, B.M., Roh, M.S., Shigemizu, D., Lichtner, P., Ishikawa, T., Aiba, T., *et al.* (2014) Novel calmodulin mutations associated

with congenital arrhythmia susceptibility. *Circ. Cardiovasc. Genet.*, **7**, 466–474.
6. Crotti, L., Johnson, C.N., Graf, E., De Ferrari, G.M., Cuneo, B.F., Ovadia, M., Papagiannis, J., Feldkamp, M.D., Rathi, S.G., Kunic, J.D., *et al.* (2013) Calmodulin mutations associated with recurrent cardiac arrest in infants. *Circulation*, **127**, 1009–1017.
7. Nyegaard, M., Overgaard, M.T., Sondergaard, M.T., Vranas, M., Behr, E.R., Hildebrandt, L.L., Lund, J., Hedley, P.L., Camm, A.J., Wettrell, G., *et al.* (2012) Mutations in calmodulin cause ventricular tachycardia and sudden cardiac death. *Am. J. Hum. Genet.*, **91**, 703–712.
8. Marsman, R.F., Barc, J., Beekman, L., Alders, M., Dooijes, D., van den Wijngaard, A., Ratbi, I., Sefiani, A., Bhuiyan, Z.A., Wilde, A.A., *et al.* (2014) A mutation in CALM1 encoding calmodulin in familial idiopathic ventricular fibrillation in childhood and adolescence. *J. Am. Coll. Cardiol.*, **63**, 259–266.
9. Shamgar, L. (2006) Calmodulin is essential for cardiac IKS channel gating and assembly: impaired function in long-QT mutations. *Circ. Res.*, **98**, 1055–1063.
10. Ciampa, E.J., Welch, R.C., Vanoye, C.G. and George, A.L. (2010) KCNE4 juxtamembrane region is required for interaction with calmodulin and for functional suppression of KCNQ1. *J. Biol. Chem.*, **286**, 4141–4149.
11. Van Petegem, F., Lobo, P.A. and Ahern, C.A. (2012) Seeing the forest through the trees: towards a unified view on physiological calcium regulation of voltage-gated sodium channels. *Biophys. J.*, **103**, 2243–2251.
12. Mori, M.X., Erickson, M.G. and Yue, D.T. (2004) Functional stoichiometry and local enrichment of calmodulin interacting with Ca2+ channels. *Science*, **304**, 432–435.
13. Yamaguchi, N., Xu, L., Pasek, D.A., Evans, K.E. and Meissner, G. (2003) Molecular basis of calmodulin binding to cardiac muscle Ca(2+) release channel (ryanodine receptor). *J. Biol. Chem.*, **278**, 23480–23486.
14. Bers, D.M. (2004) Macromolecular complexes regulating cardiac ryanodine receptor function. *J. Mol. Cell Cardiol.*, **37**, 417–429.
15. Sorensen, A.B., Sondergaard, M.T. and Overgaard, M.T. (2013) Calmodulin in a heartbeat. *febs J.*, **280**, 5511–5532.
16. Budde, T., Meuth, S. and Pape, H.C. (2002) Calcium-dependent inactivation of neuronal calcium channels. *Nat. Rev. Neurosci.*, **3**, 873–883.
17. Moretti, A., Bellin, M., Welling, A., Jung, C.B., Lam, J.T., Bott-Flugel, L., Dorn, T., Goedel, A., Hohnke, C., Hofmann, F., *et al.* (2010) Patient-specific induced pluripotent stem-cell models for long-QT syndrome. *N. Engl J. Med.*, **363**, 1397–1409.
18. Muller, M., Seufferlein, T., Illing, A. and Homann, J. (2013) Modelling human channelopathies using induced pluripotent stem cells: a comprehensive review. *Stem Cells Int.*, **2013**, 496501.
19. Yazawa, M., Hsueh, B., Jia, X., Pasca, A.M., Bernstein, J.A., Hallmayer, J. and Dolmetsch, R.E. (2011) Using induced pluripotent stem cells to investigate cardiac phenotypes in Timothy syndrome. *Nature*, **471**, 230–234.
20. Kaese, S., Frommeyer, G., Verheule, S., van Loon, G., Gehrmann, J., Breithardt, G. and Eckardt, L. (2013) The ECG in cardiovascular-relevant animal models of electrophysiology. *Herzschrittmacherther Elektrophysiol.*, **24**, 84–91.
21. Janse, M.J., Opthof, T. and Kleber, A.G. (1998) Animal models of cardiac arrhythmias. *Cardiovasc. Res.*, **39**, 165–177.
22. Okita, K., Yamakawa, T., Matsumura, Y., Sato, Y., Amano, N., Watanabe, A., Goshima, N. and Yamanaka, S. (2013) An efficient nonviral method to generate integration-free human-induced pluripotent stem cells from cord blood and peripheral blood cells. *Stem Cells*, **31**, 458–466.
23. Takahashi, K., Tanabe, K., Ohnuki, M., Narita, M., Ichisaka, T., Tomoda, K. and Yamanaka, S. (2007) Induction of pluripotent stem cells from adult human fibroblasts by defined factors. *Cell*, **131**, 861–872.
24. Nakagawa, M., Koyanagi, M., Tanabe, K., Takahashi, K., Ichisaka, T., Aoi, T., Okita, K., Mochiduki, Y., Takizawa, N. and Yamanaka, S. (2008) Generation of induced pluripotent stem cells without Myc from mouse and human fibroblasts. *Nat. Biotechnol.*, **26**, 101–106.
25. Yang, L., Soonpaa, M.H., Adler, E.D., Roepke, T.K., Kattman, S.J., Kennedy, M., Henckaerts, E., Bonham, K., Abbott, G.W., Linden, R.M., *et al.* (2008) Human cardiovascular progenitor cells develop from a KDR+ embryonic-stem-cell-derived population. *Nature*, **453**, 524–528.
26. Matsa, E., Rajamohan, D., Dick, E., Young, L., Mellor, I., Staniforth, A. and Denning, C. (2011) Drug evaluation in cardiomyocytes derived from human induced pluripotent stem cells carrying a long QT syndrome type 2 mutation. *Eur. Heart J.*, **32**, 952–962.
27. Burridge, P.W., Matsa, E., Shukla, P., Lin, Z.C., Churko, J.M., Ebert, A.D., Lan, F., Diecke, S., Huber, B., Mordwinkin, N.M., *et al.* (2014) Chemically defined generation of human cardiomyocytes. *Nat. Methods*, **11**, 855–860.
28. Doss, M.X., Di Diego, J.M., Goodrow, R.J., Wu, Y., Cordeiro, J.M., Nesterenko, V.V., Barajas-Martinez, H., Hu, D., Urrutia, J., Desai, M., *et al.* (2012) Maximum diastolic potential of human induced pluripotent stem cell-derived cardiomyocytes depends critically on I(Kr). *PLoS One*, **7**, e40288.
29. Cordeiro, J.M., Nesterenko, V.V., Sicouri, S., Goodrow, R.J., Jr., Treat, J.A., Desai, M., Wu, Y., Doss, M.X., Antzelevitch, C. and Di Diego, J.M. (2013) Identification and characterization of a transient outward K+ current in human induced pluripotent stem cell-derived cardiomyocytes. *J. Mol. Cell Cardiol.*, **60**, 36–46.
30. Peersen, O.B., Madsen, T.S. and Falke, J.J. (1997) Intermolecular tuning of calmodulin by target peptides and proteins: differential effects on Ca2+ binding and implications for kinase activation. *Protein Sci.*, **6**, 794–807.
31. Hwang, H.S., Nitu, F.R., Yang, Y., Walweel, K., Pereira, L., Johnson, C.N., Faggioni, M., Chazin, W.J., Laver, D., George, A.L., Jr., *et al.* (2014) Divergent regulation of ryanodine receptor 2 calcium release channels by arrhythmogenic human calmodulin missense mutants. *Circ. Res.*, **114**, 1114–1124.
32. Peterson, B.Z., DeMaria, C.D., Adelman, J.P. and Yue, D.T. (1999) Calmodulin is the Ca2+ sensor for Ca2+ -dependent inactivation of L-type calcium channels. *Neuron*, **22**, 549–558.
33. Kim, J., Ghosh, S., Liu, H., Tateyama, M., Kass, R.S. and Pitt, G.S. (2004) Calmodulin mediates Ca2+ sensitivity of sodium channels. *J. Biol. Chem.*, **279**, 45004–45012.
34. Limpitikul, W.B., Dick, I.E., Joshi-Mukherjee, R., Overgaard, M.T., George, A.L., Jr. and Yue, D.T. (2014) Calmodulin mutations associated with long QT syndrome prevent inactivation of cardiac L-type Ca(2+) currents and promote proarrhythmic behavior in ventricular myocytes. *J. Mol. Cell Cardiol.*, **74**, 115–124.
35. Sondergaard, M.T., Tian, X., Liu, Y., Wang, R., Chazin, W.J., Chen, S.R. and Overgaard, M.T. (2015) Arrhythmogenic calmodulin mutations affect the activation and termination of cardiac ryanodine receptor-mediated Ca2+ release. *J. Biol. Chem.*, **290**, 26151–26162.
36. Shah, V.N., Wingo, T.L., Weiss, K.L., Williams, C.K., Balser, J.R. and Chazin, W.J. (2006) Calcium-dependent regulation of

the voltage-gated sodium channel hH1: intrinsic and extrinsic sensors use a common molecular switch. *Proc. Natl Acad. Sci. U S A*, **103**, 3592–3597.
37. Yin, G., Hassan, F., Haroun, A.R., Murphy, L.L., Crotti, L., Schwartz, P.J., George, A.L. and Satin, J. (2014) Arrhythmogenic calmodulin mutations disrupt intracellular cardiomyocyte Ca2+ regulation by distinct mechanisms. *J. Am. Heart Assoc.*, **3**, e000996.
38. Ghosh, S., Nunziato, D.A. and Pitt, G.S. (2006) KCNQ1 assembly and function is blocked by long-QT syndrome mutations that disrupt interaction with calmodulin. *Circ. Res.*, **98**, 1048–1054.
39. Vinogradova, T.M., Zhou, Y.Y., Bogdanov, K.Y., Yang, D., Kuschel, M., Cheng, H. and Xiao, R.P. (2000) Sinoatrial node pacemaker activity requires Ca(2+)/calmodulin-dependent protein kinase II activation. *Circ. Res.*, **87**, 760–767.
40. Rigg, L., Mattick, P.A., Heath, B.M. and Terrar, D.A. (2003) Modulation of the hyperpolarization-activated current (I(f)) by calcium and calmodulin in the guinea-pig sino-atrial node. *Cardiovasc. Res.*, **57**, 497–504.
41. Horii, T., Tamura, D., Morita, S., Kimura, M. and Hatada, I. (2013) Generation of an ICF syndrome model by efficient genome editing of human induced pluripotent stem cells using the CRISPR system. *Int. J. Mol. Sci.*, **14**, 19774–19781.
42. Merkle, F.T., Neuhausser, W.M., Santos, D., Valen, E., Gagnon, J.A., Maas, K., Sandoe, J., Schier, A.F. and Eggan, K. (2015) Efficient CRISPR-Cas9-mediated generation of knockin human pluripotent stem cells lacking undesired mutations at the targeted locus. *Cell Rep.*, **11**, 875–883.
43. Ye, L., Wang, J., Beyer, A.I., Teque, F., Cradick, T.J., Qi, Z., Chang, J.C., Bao, G., Muench, M.O., Yu, J., *et al.* (2014) Seamless modification of wild-type induced pluripotent stem cells to the natural CCR5Delta32 mutation confers resistance to HIV infection. *Proc. Natl. Acad. Sci. U S A*, **111**, 9591–9596.
44. Li, H.L., Fujimoto, N., Sasakawa, N., Shirai, S., Ohkame, T., Sakuma, T., Tanaka, M., Amano, N., Watanabe, A., Sakurai, H., *et al.* (2015) Precise correction of the dystrophin gene in Duchenne muscular dystrophy patient induced pluripotent stem cells by TALEN and CRISPR-Cas9. *Stem Cell Reports*, **4**, 143–154.
45. Firth, A.L., Menon, T., Parker, G.S., Qualls, S.J., Lewis, B.M., Ke, E., Dargitz, C.T., Wright, R., Khanna, A., Gage, F.H., *et al.* (2015) Functional gene correction for cystic fibrosis in lung epithelial cells generated from patient iPSCs. *Cell Rep.*, **12**, 1385–1390.
46. Fu, Y., Foden, J.A., Khayter, C., Maeder, M.L., Reyon, D., Joung, J.K. and Sander, J.D. (2013) High-frequency off-target mutagenesis induced by CRISPR-Cas nucleases in human cells. *Nat. Biotechnol.*, **31**, 822–826.
47. Hsu, P.D., Scott, D.A., Weinstein, J.A., Ran, F.A., Konermann, S., Agarwala, V., Li, Y., Fine, E.J., Wu, X., Shalem, O., *et al.* (2013) DNA targeting specificity of RNA-guided Cas9 nucleases. *Nat. Biotechnol.*, **31**, 827–832.
48. Shen, B., Zhang, W., Zhang, J., Zhou, J., Wang, J., Chen, L., Wang, L., Hodgkins, A., Iyer, V., Huang, X., *et al.* (2014) Efficient genome modification by CRISPR-Cas9 nickase with minimal off-target effects. *Nat. Methods*, **11**, 399–402.
49. Limpitikul, W.B., Dick, I.E., Tester, D., Boczek, N.J., Limphong, P., Yang, W., Choi, M.H., Babich, J., DiSilvestre, D., Kanter, R.J., *et al.* (2016) A precision medicine approach to the rescue of function on malignant calmodulinopathic long QT syndrome. *Circ. Res.*, **120**, 39–48.
50. Nelson, C.E., Hakim, C.H., Ousterout, D.G., Thakore, P.I., Moreb, E.A., Castellanos Rivera, R.M., Madhavan, S., Pan, X., Ran, F.A., Yan, W.X., *et al.* (2016) In vivo genome editing improves muscle function in a mouse model of Duchenne muscular dystrophy. *Science*, **351**, 403–407.
51. Tabebordbar, M., Zhu, K., Cheng, J.K., Chew, W.L., Widrick, J.J., Yan, W.X., Maesner, C., Wu, E.Y., Xiao, R., Ran, F.A., *et al.* (2016) In vivo gene editing in dystrophic mouse muscle and muscle stem cells. *Science*, **351**, 407–411.
52. Ran, F.A., Hsu, P.D., Wright, J., Agarwala, V., Scott, D.A. and Zhang, F. (2013) Genome engineering using the CRISPR-Cas9 system. *Nat. Protoc.*, **8**, 2281–2308.